

Combustion Characteristics for Assisted Air Pressure Swirl Atomizer

Hamada Mohamed Gad⁽¹⁾, Eslam Baraya⁽²⁾, Tharwat Messiha⁽³⁾, Ibrahim Abdelrahman⁽⁴⁾

Associate Professor Mechanical Power Engineering Department, Faculty of Engineering, Port Said University, Port Said, Egypt⁽¹⁾

Department of Mechanical Power Engineering, Faculty of Engineering, Port Said University, Port-Said, Egypt⁽²⁾

Professor Department of Mechanical Power Engineering, Faculty of Engineering, Port Said University, Port-Said, Egypt⁽³⁾

Associate Professor Mechanical Power Engineering Department, Faculty of Engineering, Port Said University, Port Said, Egypt⁽⁴⁾

ARTICLE INFO

Article history:

Received:

Accepted:

Online:

Keywords:

Pressure swirl atomizer

Air assist

Swirl passage size

Combustion characteristics

ABSTRACT

The present study is focused on studying the combustion characteristics of the modified pressure-swirl atomizers (PSA) to operate as air assist pressure swirl atomizer (AAPSA) under different operating conditions and different sizes of the atomizer swirl passage (width x depth). The new design of the atomizer is considered to operate either as pressure swirl or air assist atomizers. The operating condition studied are air to fuel mass ratio which changed as 27, 37, 52 and 65, assist air mass flow rate which varied as 3, 4, 5 and 7.5 g/s, the input thermal load which changed as 27, 44, 60, and 80 kW. The atomizer swirl passages sizes are varied as 1x1, 1.5x1.5, 2x2 and 2.5x2.5 mm². Combustion test rig is designed and manufactured to investigate the effects of the above parameters on the combustion characteristics. The temperatures maps, dimensionless visible flame length and combustion species concentrations along the combustor are measured and presented using commercial diesel oil as fuel. The results indicate that, by increasing the swirl passage size, the high temperatures region size increased, the visible flame length increased, CO and O₂ concentrations increased, while NO and CO₂ concentrations decreased. The axial NO concentrations trend is matched with the axial flame temperature profile. The flame length increased by increasing assist air mass flow rate, thermal load, swirl passage size and by decreasing the air to fuel ratio.

1. Introduction

Pressure swirl atomizer has good performance but requires high reliable fuel pump provide the fuel at high pressure to enhance the spray characteristics [1]. Pressure swirl atomizer were widely used in aircraft and internal combustion engines because of their inherent simplicity, high atomization performance, and reliable combustion stability. Pressure swirl atomizers have many advantages over other atomizer types, simply constructed, low cost, and high reliability [2-8].

Zheng et al. [9] experimentally studied the spray characteristics of the pressure swirl nozzle using particle dynamics analysis and high-speed photography system, specifically focusing on the dependence of geometrical dimensions of orifice on the spray Sauter mean diameter, velocity magnitude, droplet concentration distribution and spray cone angle.

Zhilin et al. [10] investigated experimentally five types of pressure swirl atomizers with different swirl chamber length, also changes the liquid fuel fed to atomizers with different liquid viscosities to indicate the effects of the swirl chamber length and the liquid viscosity on the air core size. The results were confirmed the results obtained in [11].

Ahmad et al. [12] studied the optimum number of tangential ports and sizes that produces widest spray and measured the air core diameter of pressure swirl atomizer. It was concluded that, increase numbers of tangential ports produce widest increasing spray and decreasing air core diameter. Reza et al. [13] studied the effect of swirling chamber length on the droplet size distributions for the pressure swirl atomizer. The results indicated

that, lowest ratio swirl chamber length to diameter ratio generates hollow-cone type spray where spray structure gradually turned to solid-cone type with increasing swirl chamber length to diameter ratio.

Gad et al. [14] experimentally studied the effect of geometrical parameters on spray characteristics of a modified pressure swirl atomizer. Xue et al. [15] investigated the effect on atomizer performance of four geometric parameters, swirl port angle, swirl chamber convergent, discharge orifice length and orifice diameter. The results indicate that, the increase in swirl port angle leads to decrease film thickness and discharge coefficient and wide spray cone angle. Gad et al. [16] experimentally examined the spray performance of air blast atomizer under different operating conditions and different internal atomizer geometry.

The combustion process within a gas turbine engine is a complex interaction between flow aerodynamics, chemical kinetics, and air-fuel mixing [17]. Experimental measurements in a horizontal, cylindrical, laboratory scale water-cooled combustor was performed by Khodir et al. [18] to understand and analyze flame characteristics of a light diesel fuel. Axial and radial inflame temperature profiles, heat flux through the water jacket and flame stability has been investigated.

Looking at the previous review, it is clearly concluded that the effects of the geometrical parameters for the pressure swirl atomizer (PSA) and air assist pressure swirl atomizer (AAPSA) on spray characteristics such as spray cone angle, breakup length, spray distribution, penetration length, spray mean diameter, and spray momentum were extensively studied. There is a lack of information about the effects of the operating conditions and

geometrical parameters on the spray combustion characteristics of the atomizer such as flame temperatures distributions, flame length, species concentrations or the flame structure.

The main objective of the present study concerns on studying the combustion characteristics of the AAPSA under different operating conditions such as air to fuel mass ratio, air assist mass flow rate, input thermal load and different sizes for the swirl passages of the atomizer. The air to fuel mass ratio (AFR) is changed from 27 to 65. The assist air mass flow rate (\dot{m}_{ass}) is introduced as 3, 4, 5 and 7.5 g/s. The input thermal load (T.L) is varied 27, 44, 60, and 80 kW. The atomizer swirl passages sizes are varied by changing the width (W) and the depth (H) of the passage and WxH takes the values of 1x1, 1.5x1.5, 2x2 and 2.5x2.5 mm². The temperatures maps which describe the axial and radial temperatures distributions, dimensionless visible flame length and combustion species concentrations along the combustor are measured and presented using commercial diesel oil as fuel.

2. Experimental Test Rig

To study the above parameters and conditions, a combustion test rig is designed and manufactured. The used combustion test rig consists of combustion airline, assist airline, liquid fuel line, burner head and a cylindrical water-cooled axisymmetric combustor. The schematic diagram of the used experimental

combustion test rig is shown in Figure 1. The combustion airline comprises of air blower, control valve, 100 mm diameter air pipe, calibrated combustion air orifice and water U-tube manometer. thermometer. The liquid fuel line consists of fuel tank, suction pipe, suction valve, and suction fuel filter, vane pump electrically driven by AC motor, delivery control valve, high-pressure flexible hose, pressure gauge and return control valve. The mass flow rate is change with variation of discharge orifice diameter and injection pressure. The flame stabilizer in the present study is the air swirler with a constant swirl number (S) of 0.87. The burner arrangement is constructed from pipe has outside diameter of 150 mm which converged at the end to 100 mm diameter with growth length of 400 mm. The air swirler of S = 0.87 is fitted to 100 mm diameter end with modified pressure swirl-type atomizer. The test section is water-cooled horizontal cylindrical steel tube of 200 mm inner diameter and 1000 mm length. The combustor is equipped on one side with 19 tapping holes of 16 mm inner diameter arranged in line along the combustor to introduce measuring probes of gas temperature and for visual observation to the flame. The axial distance between the adjacent taps along the combustor is 50 mm. A double concentric jet burner is fitted axially at the up-stream end of the test section in which air swirler could be mounted at its outlet.

- | | | | | |
|---------------------|-----------------------|------------------------|------------------|------------------------------|
| 1 Air blower | 6 Air swirler | 11 Air rotameter | 16 Fuel pump | 21 Return line control valve |
| 2 Air control valve | 7 Combustor | 12 Air control valve | 17 Coupling | 22 Fuel tank |
| 3 U-tube manometer | 8 Thermometer | 13 Fuel pressure gauge | 18 AC motor | 23 Vent |
| 4 Burner head | 9 Air valve | 14 Fuel filter | 19 Control valve | 24 Blow-off valve |
| 5 Atomizer | 10 Air pressure gauge | 15 Non-return valve | 20 Fuel filter | 25 Fuel level indicator |

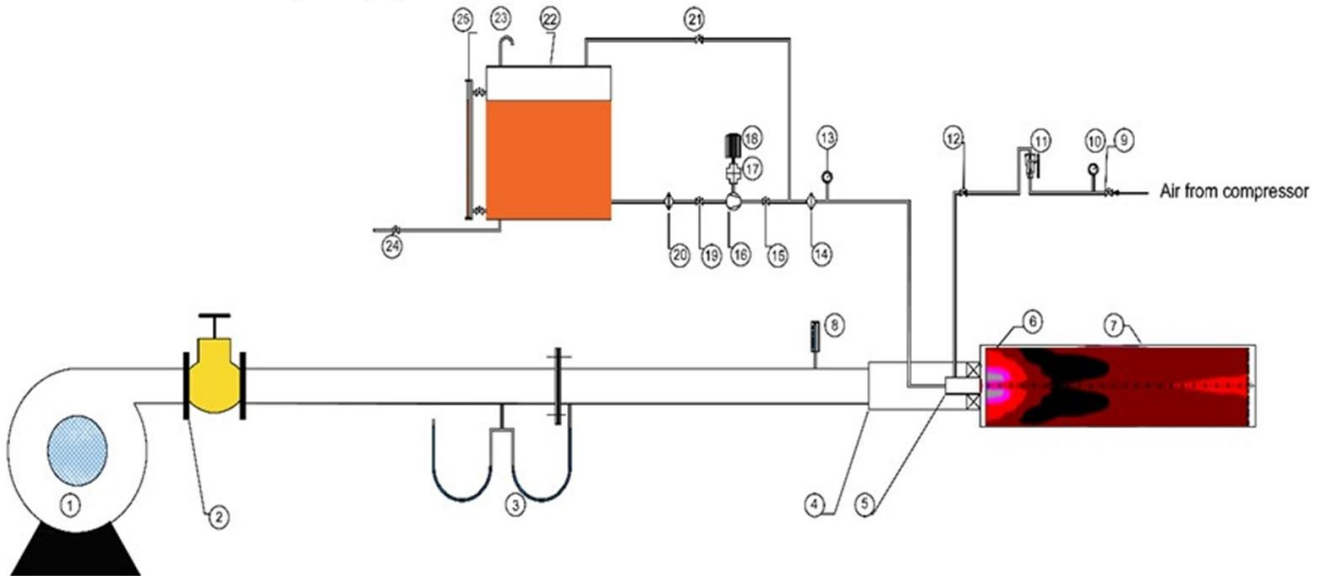


Figure 1: Schematic diagram of the experimental combustion test rig

The new design of pressure swirl atomizer is manufactured with air assist needle to overcome the defects of pressure swirl atomizer. Pressure swirl atomizer require fuel pump to give high pressure and stand by pump with same category if orifice diameter of atomizer increase to still develop good spray performance thus pressure swirl atomizer have orifice diameter limitation for fuel pump also increase of atomizing pressure

increasing cone angle. To overcome this defect, assist air is used to operate two main functions; helping to get good spray performance with large orifice area, low pressure fuel pump, large annulus orifice area and increase cone angle of developed spray. Assist air controls droplet size reduces droplet size and break up length. Assist air is entering in the middle of the atomizer through air needle at center of swirl chamber thus the

fuel exit at annulus area around air needle. Assist air needle is penetrates the swirl chamber and thus, spin chamber size was reduced, therefore air needle should have lower diameter as possible. The air needle size is subtracting from the size of swirl chamber and reduces the radius of rotation of fuel, which reduces the angler momentum of fuel entering swirl chamber. In addition, increase the angler momentum at exit due to large annuls area.

Figure 2 shows the detailed dimensions of the modified pressure swirl atomizer. The modified atomizer is consisting of main five parts; (1) atomizer body, (2) locking part to swirl fuel passage, (3) swirling part of fuel with different angles, (4) atomizer cap with different orifice diameters which contains spin chamber with cylindrical geometry and (5) central air needle. In the present work, liquid is issued from annulus area around the air needle with swirling motion. The red color refers to the liquid fuel and the blue color refers to the assist air. The orifice length to diameter ratio (L_o/D_o) and swirl chamber length/diameter ratio (L_s/D_s) are kept constants as 0.25 and 0.93, respectively.

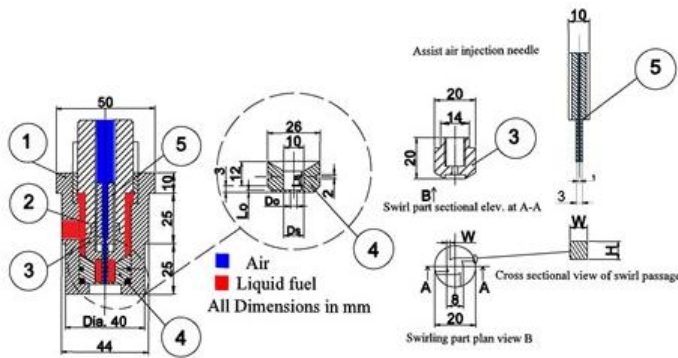


Figure 2: Detailed dimensions of the air assist pressure swirl atomizer

3. Experimental Results and Discussion

In this section the experimental results of the combustion characteristics such as temperatures distributions, dimensionless visible flame length along the combustor tube and species concentrations are measured and represented.

Combustion performance of the assisted air pressure swirl atomizer (AAPSA) is investigated for various operating and geometrical conditions. Combustion air to fuel mass ratio (AFR) is varied from 27 to 65, assisted air mass flow rate is changed from 3 to 7.5 g/s, and the input thermal load varied as 27, 44, 60 and 80 kW. Geometrical parameter of AAPSA swirl passages (width x depth) $W \times H$ which varied as 1×1 , 1.5×1.5 , 2×2 and 2.5×2.5 mm². The temperatures maps, radial and axial temperatures distributions, dimensionless visible flame length and combustion centerline species concentrations along the combustor tube are measured and studied for the above different operating and geometrical conditions using commercial diesel oil as fuel.

3.1. Temperatures patterns

The temperatures distributions inside the flame are one of the important fundamental quantities by means of which a complete detailed study can be obtained of controlling the flow behavior

from the point of view of heat transfer and combustion in industrial furnaces and combustion chambers. In the present work, the local mean temperature is measured using thermocouple. The used thermocouple is type R which consists of a Platinum-Platinum / Rhodium (13 %) bare wire thermocouple [19-20]. The used thermocouple of wire of 0.3 mm diameter. The radial temperatures are measured using the thermocouple by inserting the thermocouple in through the measuring ports to the flame centerline to measure its temperature. The thermocouple is shifted radially by increment of 1 cm to measure the radial flame temperatures at certain axial distance. The axial flame temperatures are measure using the thermocouple in the different axial ports located along the combustor.

The radial and axial temperatures distributions through the combustor tube are investigated. From the radial and the axial temperatures profiles, the temperatures maps could be drawn at any operating conditions by the help of EXCEL software program. The mean axial and radial temperature profiles along the combustor tube for all chosen operation conditions are presented. The temperatures map is described by seven regions; each region has a range of temperatures described by a certain color. The effects of assisted air mass flow rate, air to fuel mass ratio, the thermal load and swirl passage dimensions of AAPSA on temperatures patterns are studied. The experimental results are carried out using the commercial diesel oil as fuel. Table 1 illustrates the average properties of the used diesel fuel. The following subsections present the influence of the studied parameters on the different profiles of temperatures patterns.

Table 1: Average properties of used Diesel fuel (Petrobel, 2015)

| Fuel property | Value | Unit |
|-------------------------------|--------|--------------------|
| Kinematic viscosity at 40 °C | 4.35 | mm ² /s |
| Density at 20 °C | 850 | kg/m ³ |
| Surface tension at 20 °C | 0.0283 | N/m |
| Carbon | 87 | Wt.% |
| Hydrogen | 13 | Wt.% |
| Cetane number | 40-55 | |
| Heating value | 45 | MJ/kg |
| Thermal conductivity at 20 °C | 0.13 | W/(m·K) |

(i) Effect of air to fuel mass ratio on temperatures patterns

The air to fuel mass ratio is increased by increasing the air mass flow rate and keeping the fuel mass flow rate constant to keep the input thermal load constant. The temperatures maps for different values of air to fuel mass ratio are shown in Figure 3. It is inferred that, there is one reaction region distinguished with high temperature values. This region is called main reaction zone and appeared around flame axis. For the small AFR of 27, the temperature level is relatively high because of the existence of the reversed hot products. A slight decrease in temperature appears at upstream section inside the flame core. The volume of this zone decreases by increasing air mass flow rate. By increasing the AFR from 27 to 65, the flame decreased in length, increased in diameter and the flame shifted upstream nearest to the burner exit. The high temperatures regions are found at $0 \leq X/D \leq 0.2$, $0 \leq X/D \leq 0.3$, $0 \leq X/D \leq 0.2$ and $0 \leq X/D \leq 0.4$ for air to fuel ratio of 65, 52, 37 and 27, respectively. For AFR of 52 and 65, the black high temperatures regions disappeared from the temperature maps

because of the increase in the combustion air mass flow rate, also the temperatures levels in the combustor tube are decreased.

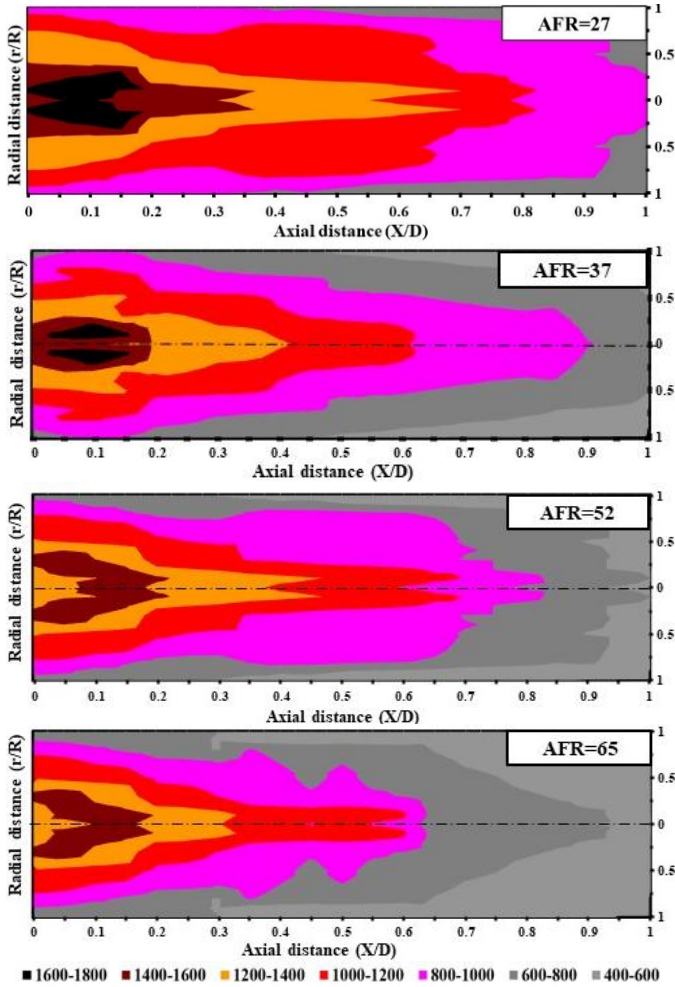


Figure 3: Effect of air to fuel mass ratio on the gas temperatures distributions with AAPSA of geometry $L_o/D_o = 0.25$, $L_s/D_s = 0.93$, $\theta = 90^\circ$ and $W \times H = 1 \times 1 \text{ mm}^2$

(ii) Effect of assist air mass flow rate on temperatures patterns

Figure 4 shows the effects of the assist air mass flow rate on the gas temperatures distributions with AAPSA of geometry $L_o/D_o = 0.25$, $L_s/D_s = 0.93$, $\theta = 90^\circ$ and $W \times H = 1 \times 1 \text{ mm}^2$. By increasing the air assist mass flow rate from 3 g/s to 7.5 g/s, the high temperature region is shifted upstream close to the burner; the flame diameter is decreased by increasing the values of the assisted air, as the spray cone angle (SCA) increased with decreasing of assisted air. The effects of the used atomizer geometric parameters on the spray characteristics especially the spray shape were presented and detailed studied by Gad et al. [14]. The present study is considered an extension for [14] for studying the combustion characteristics for the modified atomizer. The increase in the evaporation rate of spray droplet in assisted air pressure swirl atomizer because of insert of assist air, i.e., injecting of assist air helps of good atomization performance and increase SCA, which are reflected in the combustion performance. By increasing the mass flow of assisted air, the assist air helps for more disintegration of liquids fuel, decreasing of SCA while

increasing of penetration length and produce less droplets the droplets Sauter Mean Diameter (SMD).

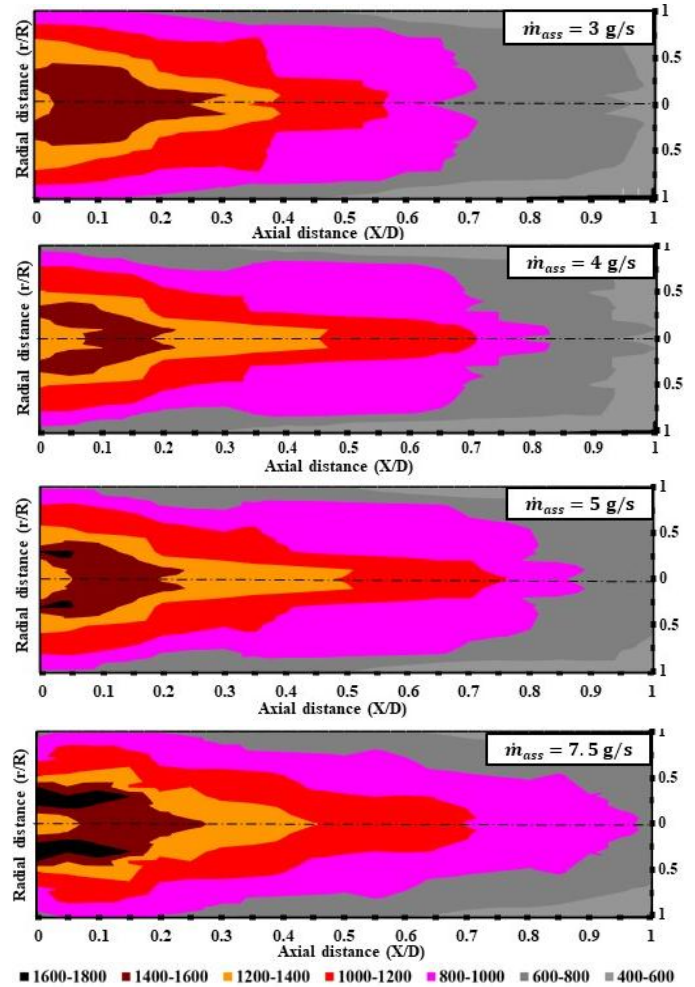


Figure 4: Effect of the assist air mass flow rate on the gas temperatures distributions at AFR = 52 for AAPSA of geometry $L_o/D_o = 0.25$, $L_s/D_s = 0.93$, $\theta = 90^\circ$ and $W \times H = 1 \times 1 \text{ mm}^2$

(iii) Effect of thermal load on temperatures patterns

The input thermal load is measured and calculated by the fuel mass flow rate (kg/s) times the caloric value or the heating value of the used fuel (kJ/kg). For changing the input thermal load, the fuel mass flow rate increased and consequently the air mass flow rate increased to keep the air to fuel mass ratio constant. Figure 5 shows the effects of changing values of the input thermal load on the gas temperatures distributions at AFR=52 for AAPSA of geometry $L_o/D_o = 0.25$, $L_s/D_s = 0.93$, $\theta = 90^\circ$. It is clearly obtained that, only one main reaction zone is formed around the flame axis, this zone increases in size by increasing the input thermal load. A relatively low temperature zone appears at upstream section around the flame centerline due to the existence of dense of fuel vapor. The volume of this zone increases by increasing thermal load input, i.e., increasing the fuel mass flow rate. Increasing the thermal load, the high temperatures region size and the flame length increased. The high temperatures regions are found at $0 \leq X/D \leq 0.75$, $0 \leq X/D \leq 0.9$, $0 \leq X/D \leq 0.9$ and $0 \leq X/D \leq 1$ for thermal loads of 27, 44, 60 and 80 kW, respectively.

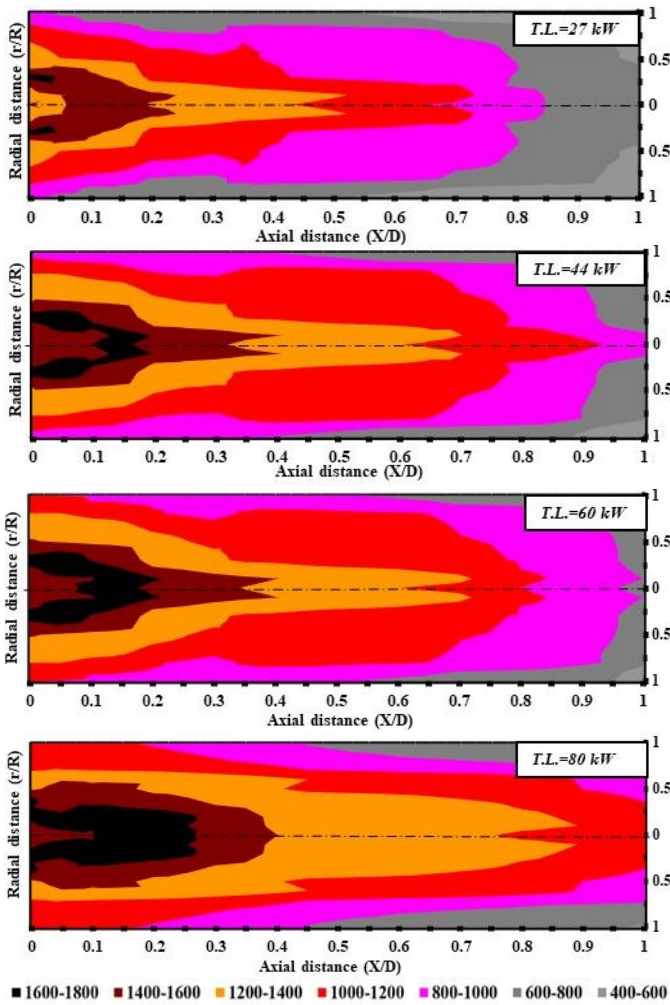


Figure 5: Effect of the thermal load on the gas temperatures distributions at AFR= 52 for AAPSA of geometry $L_o/D_o = 0.25$, $L_s/D_s = 0.93$, $\phi = 90^\circ$

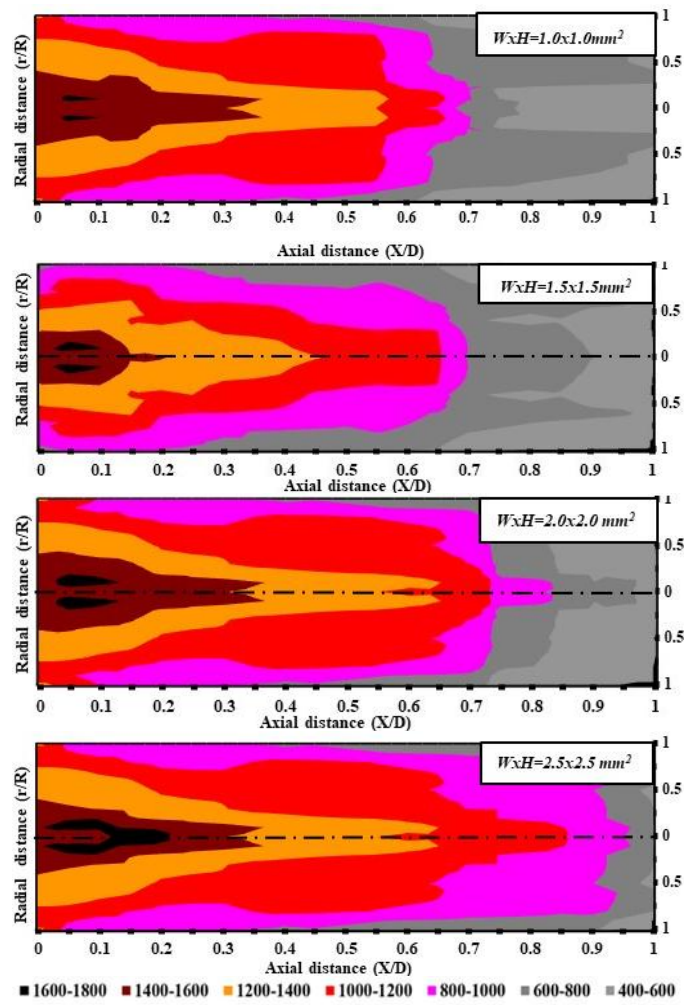


Figure 6: Effect the swirl passages size on the gas temperatures distributions at AFR=37 for AAPSA of geometry $L_o/D_o = 0.25$, $L_s/D_s = 0.93$, $\phi = 90^\circ$

(iv) Effect of swirl passages size on temperatures patterns

In the present study, the size of the swirl passages is change in width and depth. The width and depth of the swirl passage take the same dimension to give a square cross sectional. Figure 6 shows the effects of changing the values of swirl passages size (width x depth) on the gas temperatures distributions at AFR=37 for AAPSA of geometry $L_o/D_o = 0.25$, $L_s/D_s = 0.93$, $\phi = 90^\circ$. By increasing the swirl passages sizes of AAPSA, the main reaction zone formed around the flame axis, increase in size by increasing the swirl port sizes. A relatively low temperature zone appears at upstream section around the flame centerline. It is appeared that, the high temperatures regions of 800 to 1000 °C are found at $0 \leq X/D \leq 0.7$, $0 \leq X/D \leq 0.75$, $0 \leq X/D \leq 0.85$ and $0 \leq X/D \leq 1$ for swirl passage sizes of 1×1 , 1.5×1.5 , 2×2 and $2.5 \times 2.5 \text{ mm}^2$, respectively. The reduction of swirl passages sizes decreases the SMD due to increasing of swirl velocity at the entrance of spin chamber, which helps to increase the swirl effects, improve the spray quality and enhance mixing process as discussed in detail in spray characteristics [14].

3.2. Dimensionless visible flame length

In the field of combustion systems, the study of flames is considered one of the main objectives. Many practical combustion applications required short and stabilized flames over a wide range of operating conditions. In this case, it is important to minimize the heat transfer from the flame to the bounding surfaces as in combustion chamber of gas turbines. Some of another combustion systems are to transfer as much as possible heat from the flame to the working medium such as in boiler furnaces. Therefore, the flame is in this case long with high heat transfer. The flame length is defined as the length of the visible part of the flame measured from the atomizer to the visible part end. In the present study, the flame length is measured visibly through the observation ports located axially along the combustor at known different distances.

(i) Effect of air to fuel mass ratio on visible flame length

The effect of the air to fuel mass ratio on dimensionless mean visible flame length at $S = 0.87$, T.L. = 27 kW, $\dot{m}_{\text{ass}} = 5 \text{ g/s}$, AAPSA of geometry $L_o/D_o = 0.25$, $L_s/D_s = 0.93$, $\phi = 90^\circ$ and $W \times H = 1 \times 1 \text{ mm}^2$ is shown in Figure 7. It is shown that, the

dimensionless mean visible flame length is decreased as the air to fuel mass ratio increased. It is noticed that, by increasing AFR from 27 to 65, the dimensionless mean flame length is reduced by about 40%. As the AFR increased, the spray cone angle increased, as well, this means that the radial velocity component of the spray droplets increases and the axial velocity decreases. Decreasing the axial velocity leads to decreasing the axial movement of the spray droplets and, hence, the spray droplets will proceed small distances inside the combustor tube to be turned from liquid into vapor and consequently be burned. Therefore, this leads to a decrease in the flame length.

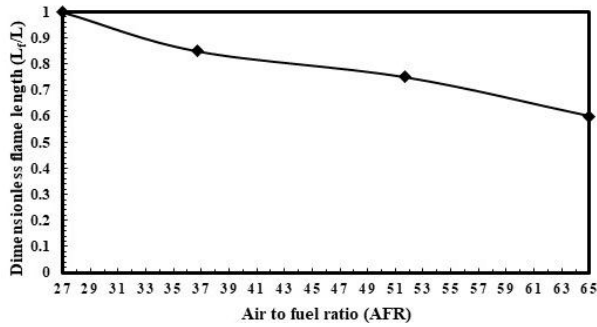


Figure 7: Effect of air to fuel mass ratio on dimensionless mean visible flame length [S = 0.87, T.L. = 27 kW, $\dot{m}_{ass} = 5$ g/s, AAPSA of geometry $L_o/D_o = 0.25$, $L_s/D_s = 0.93$, $\theta = 90^\circ$ and $W \times H = 1 \times 1$ mm²]

(ii) Effect of assisted air on visible flame length

The effects of changing the values of the assisted air mass flow rate on dimensionless visible flame length at S = 0.87, T.L. = 27 kW, AAPSA of geometry $L_o/D_o = 0.25$, $L_s/D_s = 0.93$, $\theta = 90^\circ$, $W \times H = 1 \times 1$ mm² and AFR = 52 is shown in Figure 8. It can be seen that; at assisted air mass flow of 7.5 g/s the longest dimensionless visible flame length is found due to the increase of assisted air which increases SCA, thus penetration length increases. The reduction percentage on dimensionless visible flame length as the assisted air mass flow rate increased from 3 g/s to 7.5 g/s is about 59%. This reduction in the flame length with the assist air mass flow rate is because the spray droplets burned early, i.e., at a shorter distance from the atomizer, and thus causing a decrease in the dimensionless visible flame length.

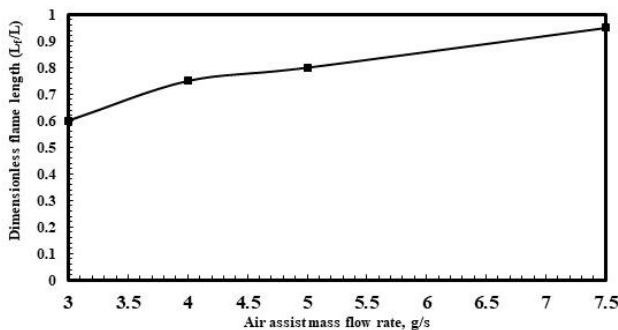


Figure 8: Effect of assisted air mass flow on dimensionless mean visible flame length at AFR = 52 [S = 0.87, T.L. = 27 kW, AAPSA of geometry $L_o/D_o = 0.25$, $L_s/D_s = 0.93$, $\theta = 90^\circ$, $W \times H = 1 \times 1$ mm²]

(iii) Effect of thermal load on visible flame length

The effect of thermal load on the dimensionless visible flame length for S = 0.87, AFR = 52, $\dot{m}_{ass} = 5$ g/s, AAPSA of geometry $L_o/D_o = 0.25$, $L_s/D_s = 0.93$, $\theta = 90^\circ$, and $W \times H = 1 \times 1$ mm² is shown in Figure 9. Increasing the thermal load, the fuel momentum is increased due to the increase in fuel velocity and fuel mass flow rate, so that, the dimensionless visible flame length increased. It is observed that, the dimensionless visible flame length increased by about 39 % when the thermal load increased from 27 to 80 kW.

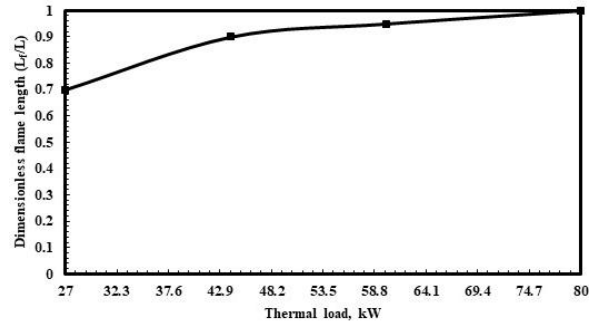


Figure 9: Effect of the input thermal load on dimensionless mean visible flame length at AFR = 52 [S = 0.87, $\dot{m}_{ass} = 5$ g/s, AAPSA of geometry $L_o/D_o = 0.25$, $L_s/D_s = 0.93$, $\theta = 90^\circ$, $W \times H = 1 \times 1$ mm²]

(iv) Effect of swirl passages size on visible flame length

The effect of swirl passages size on the dimensionless visible flame length for S = 0.87, T.L. = 27 kW, AFR = 37, $\dot{m}_{ass} = 5$ g/s, AAPSA of geometry $L_o/D_o = 0.25$, $L_s/D_s = 0.93$, $\theta = 90^\circ$ is shown in Figure 10. By increasing the swirl passages size, the spray quality is improved, the spray cone angle is reduced, and the penetration length is increased. The fuel velocity at entry of spin chamber is increased, so that, the dimensionless visible flame length is decreased because of increase of SCA. It is shown that, the dimensionless visible flame length is increased by increasing swirl passages size from $W \times H = 1 \times 1$ to 2.5×2.5 mm² by about 46 %. The liquid tangential velocity at the entry of the spin chamber is converted into angular motion in spin chamber producing low swirl effect by increasing swirl passages size and reduced spray cone angle. The liquid jet enters the spin chamber with high velocity at small dimension of swirl passages size, then SCA increased produce thin film thickness by decreasing swirl passages size resulting a decrease in dimensionless visible flame length.

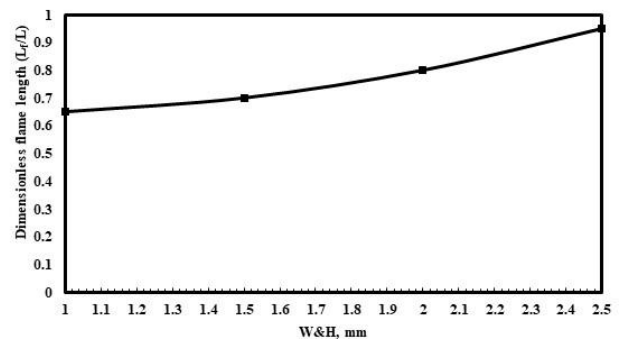


Figure 10: Effect the swirl passages size on dimensionless mean visible flame length at AFR = 37 [S = 0.87, T.L. = 27 kW, $\dot{m}_{ass} = 5$ g/s, AAPSA of geometry $L_o/D_o = 0.25$, $L_s/D_s = 0.93$, $\theta = 90^\circ$]

3.3. Species concentrations

The species concentration is measured axially through the cylindrical water-cooled combustor center line and radially at the combustor tube end using the infrared AO2000 series gas analyzer. Advanced Optima Uras 26 for CO₂, CO and NO measurements measure the species concentrations and by Magnos 206 for O₂ measurement. The maximum uncertainties are 0.5%, 1%, 1 ppm and 3 ppm for O₂, CO₂, CO, and NO, respectively.

(i) Effect of air fuel mass ratio on species concentrations

The centerline axial species concentrations for different air to fuel mass ratio is shown in Figure 11. It is found that by moving axially downstream of the combustor tube, the concentrations of CO, CO₂ and NO are decreased while the concentration of O₂ is increased. The peak concentration values of NO values close to the high temperature zone. The concentration is decreased gradually to the end of the combustor tube. By increasing the values of the air to fuel mass ratio, the disintegration process is improved which leads to an enhancement of fuel combustion reaction. This leads to an increase in fuel oxidation, which means that some of the CO will be converted to CO₂ accompanied with more release of heat energy from the combustion chemical reactions. Increasing the heat released from the combustion process raises the temperatures of the flame, which leads to an increase of the NO formation. Increasing the air to fuel mass ratio decreases the CO concentrations in flame upstream while increases the O₂ concentrations. For higher air to fuel mass ratio, increasing the axial center line O₂ and CO concentrations downstream through the flame is due to the high air velocity which causes imperfect mixing between fuel and air.

[b] AFR = 65

Figure 11: The axial species concentrations for different air to fuel mass ratios [S = 0.87, T.L. = 27 kW, $\dot{m}_{ass}=5$ g/s, AAPSA of geometry $L_o/D_o = 0.25$, $L_s/D_s=0.93$, $\theta = 90^\circ$ and $W \times H = 1 \times 1$ mm²]

Figure 12 shows the axial centerline NO concentrations and gas temperatures profiles at air to fuel mass ratio of 65. It can be seen that, both NO and gas temperature curves have the same trend, and the maximum of NO concentrations are occurred at the same position where the maximum temperature takes place. This indicates that, the thermal NO mechanism is predominant one according to Zeldovich mechanism that describes the oxidation of nitrogen and NOx formation.

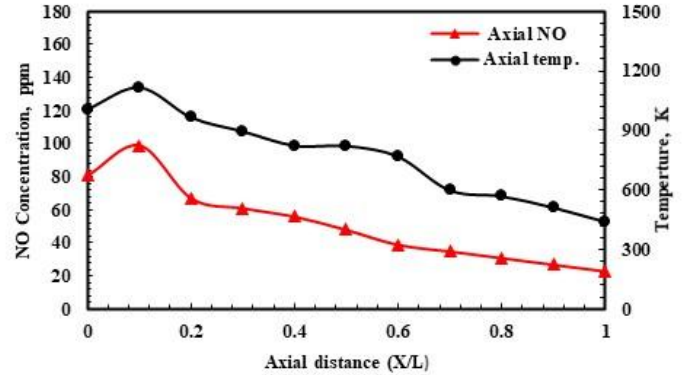


Figure 12: Centerline axial NO concentrations and gas temperatures profiles [S = 0.87, T.L. = 27 kW, AFR= 65, $\dot{m}_{ass} = 5$ g/s, AAPSA of geometry $L_o/D_o = 0.25$, $L_s/D_s=0.93$, $\theta = 90^\circ$ and $W \times H = 1 \times 1$ mm²]

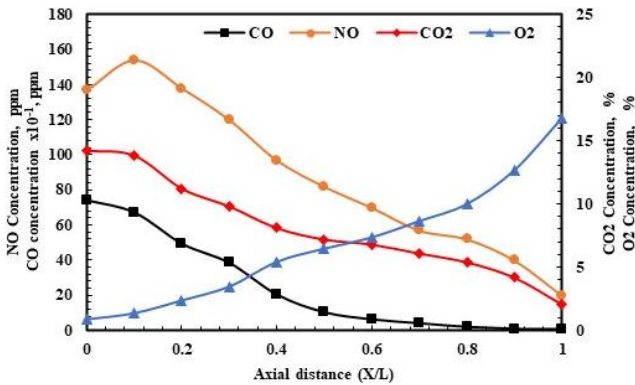
(ii) Effect of assisted air mass flow on species concentrations

The axial centerline species concentrations effect for different values of assisted air mass flow rate are shown in Figure 13. It is appeared that, the CO concentration at mass flow rate of 7.5 g/s is decreased until it disappeared at X/L=0.2 of the axial length, on the contrary at mass flow rate of 3 g/s, the CO concentrations are increased because of poor disintegration of liquid at low mass flow rate of assisted air producing low percentage of CO₂ due incomplete combustion of atomizing fuel and low quality of atomization process. NO concentrations are increased with reduction of mass flow rate of assist air due to low spray characteristics at low mass flow of assist air. The O₂ concentrations are increased at the end of combustor at assist air mass flow of 3 g/s than 7.5 g/s because of less mixing and poor demand of oxygen in chemical combustion with low mass flow of assist air.

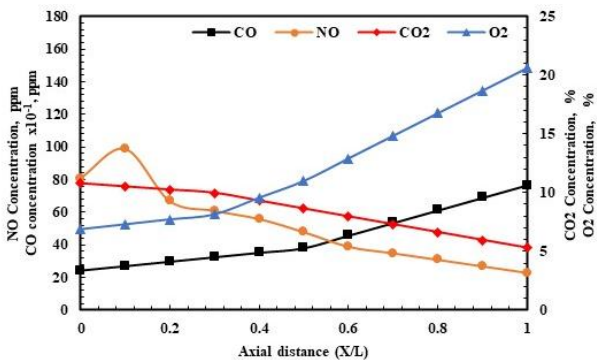
Figure 14 shows axial centerline NO concentrations and gas temperatures profiles. It can be seen that, both have the same trend, and the maximum of NO concentration is occurred at the same position where the maximum temperature takes place. The peak concentration values of NO values close to the high temperature zone then the concentration of NO is decreased gradually to the end of the combustor.

iii) Effect of thermal load on species concentrations

Increasing of thermal load at constant air to fuel ratio, the flame temperature increased, also NO increased. The effect of the



[a] AFR = 27



thermal load on the species concentrations (NO, CO, CO₂ and O₂) for air swirl number of 0.87, air to fuel mass ratio of 52 and thermal loads of 27 and 80 kW is shown in Figure 15. Increasing thermal load, NO, CO and CO₂ increased, but O₂ decreased. For air to fuel mass ratio of 52, by increasing the thermal load from 27 to 80 kW, NO, CO₂ while CO increased by about 58%, 40%, 47%, respectively, and O₂ decreased by about 8%. By increasing thermal load from 27 to 80 kW the concentrations of O₂ and CO are increased while NO and CO₂ are decreased.

Figure 16 shows the centerline axial NO concentrations and gas temperature profiles for input thermal load of 27 kW. It can be appeared that, the NO concentrations are raised sharply to reach its peak coincide with the maximum temperature region then begin to be decreased gradually towards the combustor end. The peak concentration values of NO close to the high temperature zone.

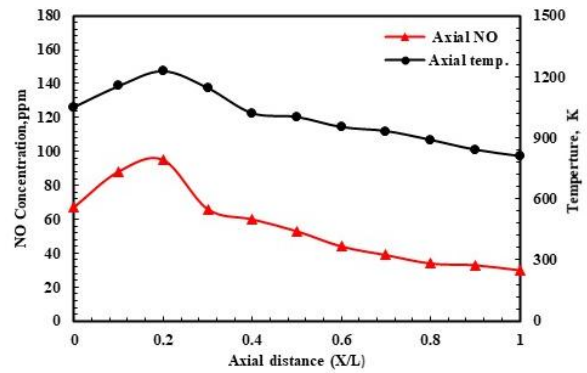
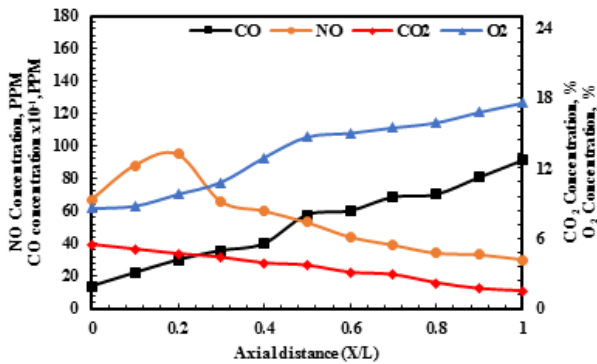
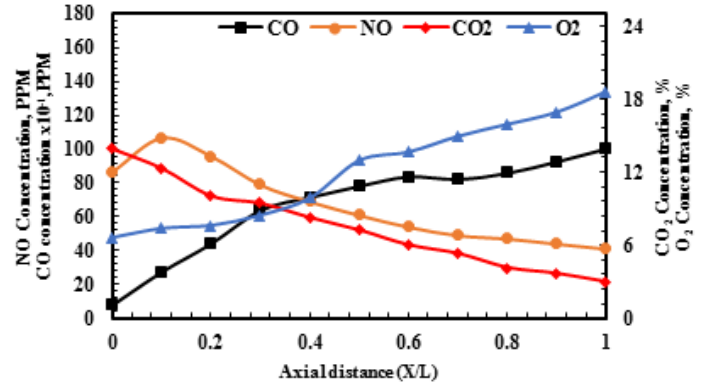


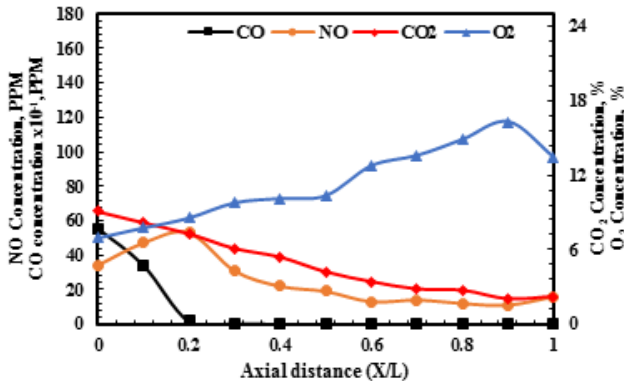
Figure 14: The axial centerline NO concentrations and gas temperature profiles [S = 0.87, AFR = 52, T.L.=27 kW, $\dot{m}_{ass} = 3 \text{ g/s}$, AAPSA of geometry $L_o/D_o = 0.25, L_s/D_s = 0.93, \theta = 90^\circ, W \times H = 1 \times 1 \text{ mm}^2$]



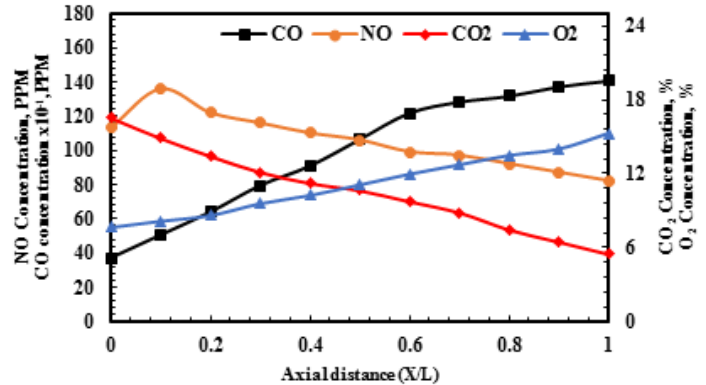
[a] $\dot{m}_{ass} = 3 \text{ g/s}$



[a] T.L.=27 kW



[b] $\dot{m}_{ass} = 7.5 \text{ g/s}$



[b] T.L.=80 kW

Figure 13: The axial species concentrations for different values of assist air mass flow at AFR = 52 [S = 0.87, T.L.=27 kW, AAPSA of geometry $L_o/D_o = 0.25, L_s/D_s = 0.93, \theta = 90^\circ, W \times H = 1 \times 1 \text{ mm}^2$]

Figure 15: The axial species concentrations for different thermal loads [S = 0.87, $\dot{m}_{ass} = 5 \text{ g/s}$, AFR = 52, AAPSA of geometry $L_o/D_o = 0.25, L_s/D_s = 0.93, \theta = 90^\circ, W \times H = 1 \times 1 \text{ mm}^2$]

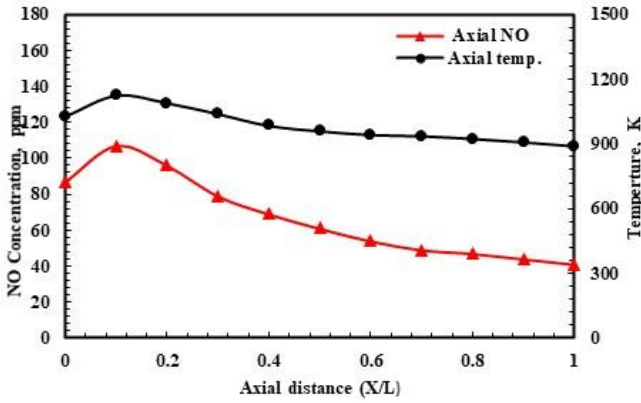
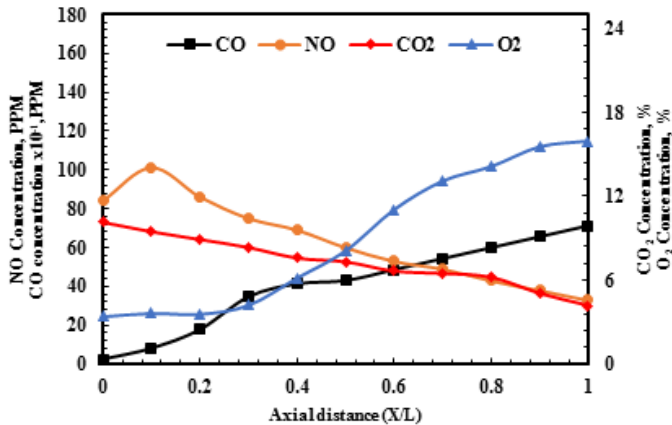


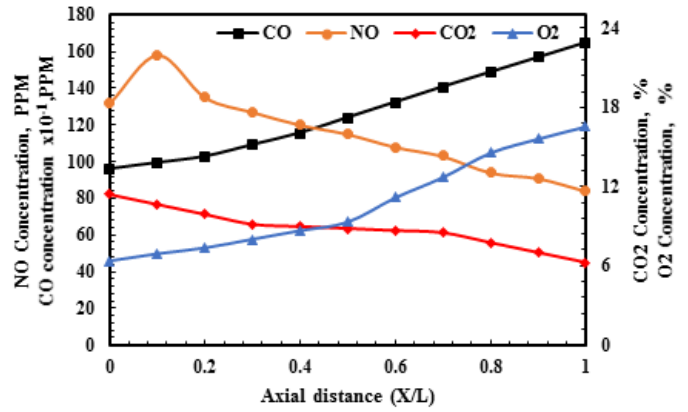
Figure 16: The axial centerline NO concentrations and gas temperature profiles [S = 0.87, $\dot{m}_{ass} = 5$ g/s, AFR = 52, T.L.=27 kW, AAPSA of geometry $L_o/D_o = 0.25$, $L_s/D_s = 0.93$, $\theta = 90^\circ$, $W \times H = 1 \times 1$ mm²]

(iv) Effect of swirl passages size on species concentrations

The axial species concentrations for different swirl passage sizes at air swirl number of 0.87 and air to fuel mass ratio of 37 is shown in Figure 17. By increasing swirl passages sizes from $W \times H = 1 \times 1$ to 2.5×2.5 mm², CO, NO and O₂ concentrations increased, while CO₂ concentrations decreased at the combustor tube exit. It is shown that, CO emission increases by increasing of $W \times H$ because of incomplete combustion due to imperfect mixing between fuel and air. When increasing the swirl passages size from $W \times H = 1 \times 1$ to 2.5×2.5 mm², NO, O₂ and CO concentrations at the combustor tube exit are increased by about 83%, 18.5%, and 211%, respectively, while CO₂ concentrations is decreased by about 55 %.



[a] $W \times H = 1 \times 1$ mm²



[b] $W \times H = 2.5 \times 2.5$ mm²

Figure 17: The axial species concentrations for different swirl passages sizes at AFR = 37 [S = 0.87, T.L. = 27 kW, $\dot{m}_{ass} = 5$ g/s, AAPSA of geometry $L_o/D_o = 0.25$, $L_s/D_s = 0.93$, $\theta = 90^\circ$]

Figure 18 shows the centerline axial NO concentrations and gas temperatures profiles for the swirl passage size of $W \times H = 2.5 \times 2.5$ mm², input thermal load of 27 kW, air to fuel mass ratio (AFR) of 37, assist air mass flow rate of 5 g/s, $L_o/D_o = 0.25$, $L_s/D_s = 0.93$, and $\theta = 90^\circ$. It is found that the center line NO concentration is increased from $X/D = 0$ to reach its maximum value because of the increasing in the center line flame temperature. It is appeared that, axial NO concentrations profiles are presented with the axial centerline flame temperatures which found to be with the same trend. This means that the thermal NO is formed in the flame envelope and the gas temperature is the most important variable which affects the NO emissions. It is clearly observed that, the peak of the center line NO concentration is found at the axial distance at where the center line peak temperature takes place, and both are found at axial distance of $X/D = 0.12$. the center line flame temperatures decrease through the flame from the peak value at $X/D = 0.12$ to its minimum value at the combustor exit and the NO concentrations take the same trend.

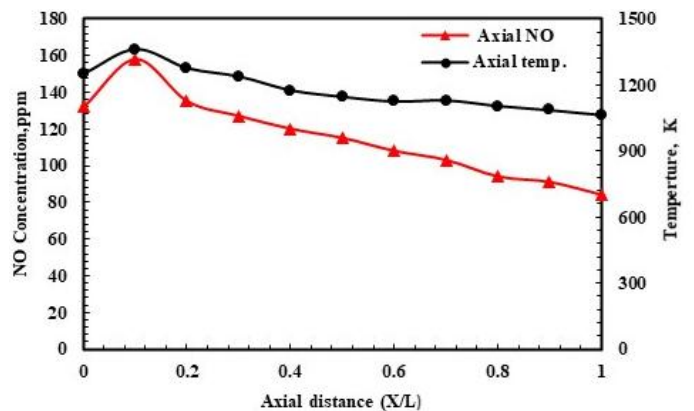


Figure 18: The axial centerline NO concentrations and gas temperature profiles [S = 0.87, T.L. = 27 kW, AFR = 37, $\dot{m}_{ass} = 5$ g/s, AAPSA of geometry $W \times H = 2.5 \times 2.5$ mm², $L_o/D_o = 0.25$, $L_s/D_s = 0.93$, $\theta = 90^\circ$]

4. Conclusions

From the experimental results by studying the spray combustion characteristics under different operating and geometrical condition for assisted air pressure swirl atomizer; air to fuel mass ratio changed as 27, 37, 52 and 65, assist air mass flow rate varied as 3, 4, 5 and 7.5 g/s, the input thermal load changed as 27, 44, 60, and 80 kW and the atomizer swirl passages varied as 1x1, 1.5x1.5, 2x2 and 2.5x2.5 mm², the following conclusions are obtained:

- The axial high temperature region is shifted upstream close to the burner and shifted outward far away from the combustor centerline by increasing the air to fuel mass ratio (AFR), while it is shifted downstream and become thinner by increasing the swirl passages sizes (WxH), input thermal load (T.L.) and decreasing of assist air mass flow rate.
- The dimensionless visible flame length is increased by increasing of assist air mass flow rate, input thermal load and swirl passages sizes, while it is decreased by increasing the AFR, the reduction in L_f/L as the assisted air mass flow rate increased from 3 g/s to 7.5 g/s is about 59%, L_f/L is increased by about 39 % as the thermal load increased from 27 to 80 kW and by about 46 % when increasing swirl passages size from $W \times H = 1 \times 1$ to 2.5×2.5 mm².
- Increasing the air to fuel mass ratio decreases the CO concentrations in flame upstream while increases the O₂ concentrations.
- By increasing the input thermal load, the centerline axial O₂ concentrations is decreased while NO, CO and CO₂ concentrations are increased.
- By increasing $W \times H$ the centerline axial O₂, NO and CO concentrations are increased while CO₂ concentration is decreased.
- By increasing the assisted air mass flow rate the centerline axial O₂ concentrations is increased while NO, CO and CO₂ concentration are decreased.
- The peak concentration value of NO is close to the high temperature zone then the concentration of NO is decreased gradually towards the end of the combustor.

Conflict of Interest

The authors declare no conflict of interest.

References

[1] Z. Ghaffar, S. Kasolang, A. Hamid and M. Rashid, "Effect of Dimensionless Numbers on Air Core Diameter of Pressure-Swirl Atomizer", Applied Mechanics and Materials, Vol. 899, 22-28, 2020. <https://doi.org/10.4028/www.scientific.net/AMM.899.22>

[2] T. Andreas and B. Günter, "Drop size spectra in sprays from pressure-swirl atomizers", International Journal of Multiphase Flow, Vol. 36, 349-363, 2010. <https://doi.org/10.1016/j.ijmultiphaseflow.2010.01.008>

[3] G. Guijun, J. W. Chang and K. Ziming, "Experimental Studies on the Spraying Pattern of a Swirl Nozzle for Coal Dust Control", Applied Science, Vol. 8, 1770, 1-14, 2018. <https://doi.org/10.3390/app8101770>

[4] H. Han, W. Pengfei, L. Ronghua, L. Yongjun, W. Jan and J. Yidan, "Experimental study on atomization characteristics of two common spiral channel pressure nozzles", The 1st International Symposium on Water Resource and Environmental Management (WREM 2018), E3S Web of Conferences, Vol. 81, No. 01022, 2019. <https://doi.org/10.1051/e3sconf/20198101022>

[5] M. Milan, S. Marcel, J. Jan, J. Lada, J. Miroslav, S. Jaroslav, and W. Graham, "Internal flow characteristics in scaled pressure-swirl atomizer", EPJ Web of Conferences, Experimental Fluid Mechanics, Vol. 180, No.02059, 2018. <https://doi.org/10.1051/epjconf/201818002059>

[6] D. Lukas, J. Jan and J. Miroslav, "Spray structure of a pressure swirl atomizer for combustion applications", European Physical Journal Conferences (EPJC), Vol. 25, No.01010, 2012. <https://doi.org/10.1051/epjconf/20122501010>

[7] M. Kamariah, O. Kahar, Y. Azli, G. Zulkifli, H. Ahmad, and K. Salmiah, "Studies on the spray characteristics of pressure-swirl atomizers for automatic hand sanitizer application", Journal of Advanced Research in Fluid Mechanics and Thermal Sciences, Vol. 55, No.1, 51-64, 2019.

[8] Y. Shanshan, Z. Ji and F. Tiegang, "Effect of viscosities on structure and instability of sprays from a swirl atomizer", Experimental Thermal and Fluid Science, Vol. 39, 58-166, 2012. <https://doi.org/10.1016/j.exptthermfluidsci.2012.01.020>

[9] Z. Huilong, L. Zhaomiao, W. Kaifeng, L. Jiayuan, L. Zexuan, "Influence of orifice geometry on atomization characteristics of pressure swirl atomizer", Science Progress, Vol. 103, No.3, 1-17, 2020. <https://doi.org/10.1177/0036850420950182>

[10] L. Zhilin, H. Yong and S. Lei, "Studies on air core size in a simplex pressure-swirl Atomizer", International Journal of Hydrogen Energy, Vol. 42, No. 29, 18649-18657, 2017. <https://doi.org/10.1016/j.ijhydene.2017.04.188>

[11] M. Pouria, N. Seyed and G. Hojat, "Experimental study of a heavy fuel oil atomization by pressure-swirl injector in the application of entrained flow gasifier", Chinese Journal of Chemical Engineering (CJOCE), Vol. 27, No.4, 765-771, 2019. <https://doi.org/10.1016/j.cjche.2018.10.001>

[12] A. Hamid, A. Rahim, N. Mohd and R. Helmi, "Spray cone angle and air core diameter of hollow cone swirl rocket injector", IIUM Engineering Journal, Special Issue, Mechanical Engineering, Vol.12, No.3, 2011. <https://doi.org/10.31436/iiumej.v12i3.66>

[13] A. Reza, V. Foad, C. Rakhul, and L. Jeekeun, "Effect of swirl chamber length on droplet size distribution in a pressure swirl atomizer", ILASS-Asia, Jeju, Korea, 2017.

[14] H.M. Gad, E.A. Baraya, T.M. Farag, and I.A. Ibrahim, "Effect of geometric parameters on spray characteristics of air assisted pressure swirl atomizer", Alexandria Engineering Journal, 61, 5557-5571, 2022. <https://doi.org/10.1016/j.aej.2021.11.010>

[15] J. Xue, M. Jog and S. Jeng, "Effect of geometric parameters on simplex atomizer performance", AIAA Journal, Vol. 42, No. 12, 2408-2415, 2004. <https://doi.org/10.2514/1.2983>

[16] H. M. Gad, I. A. Ibrahim, M. E. Abdel-baky, A. K. Abd El-samed and T. M. Farag, "Experimental study of diesel fuel atomization performance of air blast Atomizer", Experimental Thermal and Fluid Science, Vol. 99, 211-218, 2018. <https://doi.org/10.1016/j.exptthermfluidsci.2018.07.006>

[17] K. Ravi, "Engine spray combustion modeling using unified spray model with dynamic mesh refinement", M. SC., Mechanical Engineering, Iowa State University, Ames, Iowa, 2009. <https://doi.org/10.31274/etd-180810-2003>

[18] A. Khodir, M. Gaber, S. El-Beherly and W. El-Askary, "Experimental Study of Flame Characteristics by Twin Fluid Air Assist Atomizer in a Cylindrical Laboratory Combustor", First International Conference (9th Conference of Sustainable Environmental Development), Menoufia, Egypt, 2017.

[19] A. M. Salman, I. A. Ibrahim, H. M. Gad and T. M. Farag, "Effects of air temperature on combustion characteristics of LPG diffusion flame", Materials science, Vol. 1008, 128-138, 2020. <https://doi.org/10.4028/www.scientific.net/MSF.1008.128>

[20] A. A. Amer, H. M. Gad, I. A. Ibrahim, S. I. Abdel-Mageed, and T. M. Farag, "Experimental Study of LPG Diffusion Flame at Elevated Preheated Air Temperatures", World Academy of Science, Engineering and Technology, International Journal of Mechanical, Aerospace, Industrial, Mechatronic and Manufacturing Engineering, Vol. 9, No.8, 2015. <https://doi.org/10.5281/zenodo.1108072>

Abbreviation and symbols

| | |
|------------------------------------|---|
| AAPSA | Air Assisted Pressure Swirl Atomizer |
| AFR | Air to Fuel Ratio |
| D_s | Spin chamber diameter, mm |
| D_o | Orifice diameter, mm |
| H | Swirl passage depth, mm |
| L | Combustor length, 100 cm |
| L_f | Visible flame length, cm |
| L_f/L | Dimensionless flame length |
| L_o | Orifice length, mm |
| L_o/D_o | Orifice length to diameter ratio |
| L_s | Spin chamber length, mm |

| | |
|------------------------|--|
| L_s/D_s | Spin chamber length to diameter ratio |
| \dot{m}_{ass} | Assist air mass flow rate, g/s |
| PSA | Pressure Swirl Atomizer |
| r | Radial distance, cm |
| R | Combustor radius, 10 cm |
| r/R | Dimensionless radial distance |
| S | Swirl number |
| SCA | Spray Cone Angle, degree |
| SMD | Sauter Mean Diameter (D_{32}), μm |
| W | Swirl passage width, mm |
| X | Axial distance, cm |
| X/L | Dimensionless axial distance |